

© The Author(s), 2021. Published by Cambridge University Press for the Arizona Board of Regents on behalf of the University of Arizona. This is an Open Access article, distributed under the terms of the Creative Commons Attribution licence (<http://creativecommons.org/licenses/by/4.0/>), which permits unrestricted re-use, distribution, and reproduction in any medium, provided the original work is properly cited.

A NEW RAMPED PYROXIDATION/COMBUSTION FACILITY AT ¹⁴CHRONO, BELFAST: SETUP DESCRIPTION AND INITIAL RESULTS

Evelyn M Keaveney*  • Gerard T Barrett*  • Kerry Allen  • Paula J Reimer 

¹⁴CHRONO Centre for Climate, the Environment and Chronology, Archaeology & Palaeoecology Building, Queen's University Belfast, 42 Fitzwilliam Street, Belfast BT9 6AX, United Kingdom

ABSTRACT. The Belfast Ramped Pyrooxidation/Combustion (RPO/RC) facility was established at the ¹⁴CHRONO Centre (Queen's University Belfast). The facility was created to provide targeted analysis of bulk material for refined chronological analysis and carbon source attribution for a range of sample types. Here we report initial RPO results, principally on background material, but also including secondary standards that are routinely analyzed at ¹⁴CHRONO. A description of our setup, methodology, and background (blank) correction method for the system are provided. The backgrounds (anthracite, spar calcite, Pargas marble) reported by the system are in excess of 35,000 ¹⁴C years BP with a mean age of 39,345 ¹⁴C years BP ($1\sigma = 36,497\text{--}43,800$ years BP, $N=44$) with $F^{14}\text{C} = 0.0075 \pm 0.0032$. Initial results for standards are also in good agreement with consensus values: TIRI-B pine radiocarbon age = 4482 ± 47 years BP ($N=13$, consensus = 4508 years BP); IAEA-C6 ANU Sucrose $F^{14}\text{C} = 1.5036 \pm 0.0034$ ($N=10$, consensus $F^{14}\text{C} = 1.503$). These initial tests have allowed problematic issues to be identified and improvements made for future analyses.

KEYWORDS: backgrounds, radiocarbon, ramped pyrooxidation, standards.

INTRODUCTION

The new Belfast Ramped Pyrooxidation/Combustion (RPO/RC) facility was set up to provide analysis of archaeological and environmental (bulk) samples. Radiocarbon dating bulk material is problematic due to samples such as sediment, soil or peat comprising multiple carbon sources (Grimm et al. 2009; Keaveney et al. 2015; van der Plicht et al. 2016; Bao et al. 2018). In addition, the presence of contamination is also an issue due to burial conditions or preservation protocols with conserved materials (Higham 2019). Bulk material often has to undergo stringent pre-treatment procedures leading to loss of material and low carbon yields. Even with these intensive methods, the date may be younger or older than expected depending on the age of the individual fractions.

The RPO/RC method (Rosenheim et al. 2008, 2013; Hemingway et al. 2017; Zigah et al. 2017; Bao et al. 2018) was developed at The National Ocean Sciences Accelerator Mass Spectrometry (NOSAMS) and the University of South Florida. With the help of colleagues from these institutions, a ramped pyrooxidation/combustion system was constructed in the ¹⁴CHRONO Centre, Queen's University Belfast, with the capability of switching between RPO and RC modes. RPO is a method that incrementally heats a bulk sample and allows for the separation of material into its composite fractions according to their thermal stability. The RPO products are then oxidized, and the resulting CO₂ is collected cryogenically by an automated valve system. The CO₂ collected is transferred under vacuum to a connected graphitization line for conversion to graphite, which is then analyzed for radiocarbon content. By using RPO, we can acquire a profile of the CO₂ produced over different temperature intervals, providing an indication of the composition of the bulk material as well as a suite of radiocarbon values from the respective individual

*Corresponding authors. Emails: e.keaveney@qub.ac.uk, g.barrett@qub.ac.uk

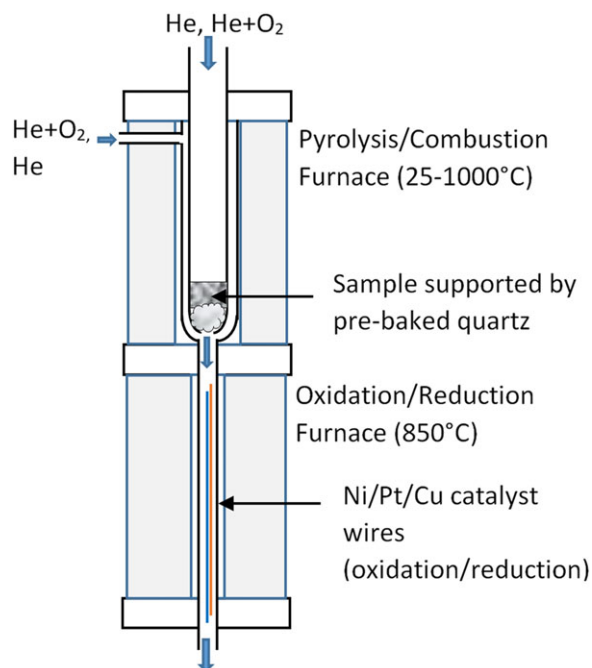


Figure 1 RPO furnace arrangement featuring upper furnace for pyrolysis or combustion of the sample and lower furnace for oxidation of pyrolysis derived products and/or reduction of oxygen from combustion process.

CO₂ fractions. Here we report initial RPO and radiocarbon analysis of background and secondary standards commonly analyzed at the ¹⁴CHRONO Centre.

METHODS

Ramped Pyrooxidation Configuration

The ramped pyrooxidation/combustion furnace arrangement is presented in Figure 1 and was designed and constructed following RPO setups used elsewhere (e.g., Rosenheim et al. 2013; Hemingway et al. 2017; Zigah et al. 2017; Bao et al. 2018). In ramped pyrooxidation mode (used in the results presented here), Helium gas (99.999% purity) flows through the top of the reactor (35 mL/min) as the sample is heated in the absence of oxygen (pyrolysis). Oxidation occurs in the lower furnace via O₂ (99.999%) that flows in (3 mL/min) through the sidearm with He (10 mL/min). This reacts with the pyrolysis derived products of the upper furnace that have been carried by helium into the lower furnace. Copper oxide, nickel and platinum (Ni/Pt/CuO) wires act as catalysts, to ensure complete oxidation of carbon-bearing pyrolysis products to CO₂.

The RPO quartz reactor insert (Figure 1) was baked at 850°C overnight, and then baked at 1000°C in-situ in the pyrolysis furnace until no CO₂ was produced. Bulk samples were lyophilised overnight and placed in the quartz reactor insert, which was then inserted to the quartz reactor vessel in the upper furnace (Figure 1). The mass of material required is dependent on carbon content but typically in the order of 20–100 mg.

The oxidation furnace was switched on and allowed to reach 850°C before the ramping furnace was set to continuously ramp to 1000°C, typically over 3–4 hr, with ramp rates in the range of 2.5–6.5°C per min, depending on sample type. Ramp rates were also varied to investigate the impact on the CO₂ profile and to examine the effect of contamination introduced for different collection time intervals. Any CO₂ evolved over the ramp cycle was quantified using a Sable Systems CA-10 infra-red CO₂ detector, and spectra were logged using LabVIEW software and National Instruments data acquisition hardware.

An automated cryogenic trap system was used to collect CO₂ from targeted areas of the spectrum. For new sample types, an initial “profile” run without collection illustrated the temperature at which intervals CO₂ structures of interest occurred. CO₂ was cryogenically captured at these intervals for radiocarbon measurement during subsequent “collection” runs. The CO₂ was transferred under vacuum to a connected (newly constructed) graphitization line, and samples were graphitized in the presence of an iron catalyst at 560°C for 4 hr using the Bosch-Manning hydrogen reduction method (Manning and Reid 1977; Vogel et al. 1987). Samples were analyzed on a 0.5 MeV National Electrostatics compact accelerator mass spectrometer (AMS) at the ¹⁴CHRONO Centre in Queen’s University Belfast. The ¹⁴C/¹²C ratio of the sample relative to an international standard (F¹⁴C) and its associated uncertainty were calculated according to Reimer et al. (2004) and van der Plicht and Hogg (2006) and incorporated a fractionation correction (Stuiver and Polach 1977) based on ¹³C/¹²C measured by AMS.

Background (Blank) Measurements

A suitable background correction for the ¹⁴CHRONO RPO system was developed based on methods used at the NOSAMS RPO Facility (Fernandez et al. 2014; Hemingway et al. 2017). Data was used from 14 separate RPO runs carried out on background materials routinely analyzed at the ¹⁴CHRONO Centre (anthracite (%C = 85–98%), sparitic calcite (%C = 12%, theoretical), and Pargas marble, all of geological age, i.e., negligible ¹⁴C content). CO₂ was collected from 38 temperature intervals. Fifty AMS radiocarbon measurements were obtained from the CO₂ produced (12 were duplicates). Two to six temperature fractions of CO₂ were isolated for each run with the median temperature of collection ranging from 601–908°C, the duration of collection ranging from 1.2 to 8.1 min, and the sampled mass ranging from 0.25 to 2 mg C. Contamination was determined in 6 samples due to inaccurate ¹⁴C dates (having a bias consistent with air leakages). These were removed from the analysis, 2 on account of leakage into the graphitization line reactors (connector issues) and 4 due to significant leakage in the RPO setup (resolved with tightening or replacement of connectors and inspection/replacement of valve seals).

Standard Measurements

A series of RPO measurements have been carried out on two standards: TIRI-B pine, which has a consensus value of 4508 ¹⁴C years BP, ¹⁴CHRONO mean value = 4507 ± 44 years BP (n = 542), %C = 47 ± 10% and IAEA-C6 ANU Sucrose with a consensus F¹⁴C = 1.503, ¹⁴CHRONO mean value = 1.503 ± 0.0078 (n = 1868), %C = 42% (theoretical). For each, 4 RPO runs were carried out as a part of initial tests of the system and newly constructed hydrogen graphitization line. For TIRI-B, a total of 20 CO₂ fractions were successfully captured and graphitized for radiocarbon dating. For Sucrose, a total of 14 gas CO₂ fractions were successfully captured, graphitized and radiocarbon dated. Usually, a series of RPO runs were carried out and dated on a wheel with other routine samples before a complete wheel of RPO samples was run on the AMS. For this reason, line leakages

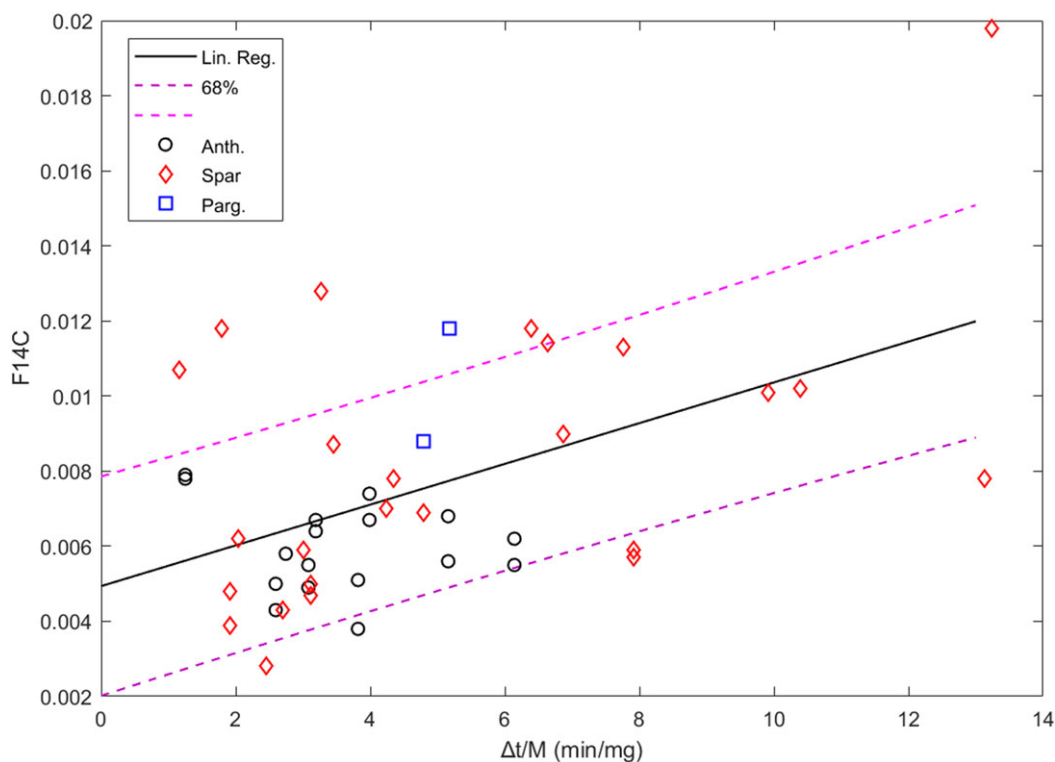


Figure 2 Linear regression plot of $F^{14}C$ versus $\Delta t/M$ for all RPO background runs. Black circle—anthracite; red diamond—spar calcite; blue square—Pargas marble. Dashed magenta—1 σ uncertainty on regression model. Regression result: $y = 0.0005 (\pm 0.0002) x + 0.0049 (\pm 0.0008)$, $R^2 = 0.25$.

affected multiple runs before being identified and resolved (radiocarbon dates on standards deviated significantly from consensus dates significantly in a direction consistent with air leakages). Four TIRI-B samples (fractions from a single RPO run) were discarded due to a RPO line leak and a further three dates were removed due to graphite line reactor leakages. Three Sucrose samples were discarded due to graphite line/separation valve line leakages, and one was discarded as a measurement outlier (using Chauvenet's criterion for outlier identification, Hughes and Hase 2009).

Background (Blank) Corrections

It is necessary to carry out a background correction for any non-background run in the system. From analysis of the background results, variation of $F^{14}C$ with RPO variables such as the ramp rate and collection temperature were not found to be statistically significant. However, there was a relationship with the quantity of CO_2 collected (expressed as mg C) and the ratio of the collection time to quantity of CO_2 collected (Figure 2). This latter variable reflects the fraction of CO_2 contamination introduced to the system through leakages in the RPO/RC line with its relationship to $F^{14}C$ derived in the background correction now described.

For an RPO measurement on background material, the measured $F^{14}C_B$, of mass M_B , is expressed as a combination of a dead component, $F^{14}C_D$, of mass M_D , and a contaminating

component, F¹⁴C_C, of mass M_C (under ideal conditions F¹⁴C_D = 0, however, in the following derivation F¹⁴C_D is used to reflect and incorporate any non-RPO/RC related deviation of the blank from zero, for example contaminant introduced to the blank prior to loading in the RPO/RC reactor). The measured F¹⁴C_B can be expressed as:

$$F^{14}C_B = F^{14}C_D \frac{M_D}{M_B} + F^{14}C_C \frac{M_C}{M_B} \tag{1}$$

with

$$M_B = M_D + M_C \tag{2}$$

Using (2) we can re-express (1) as

$$F^{14}C_B = F^{14}C_D + \frac{M_C}{M_B} (F^{14}C_C - F^{14}C_D) \tag{3}$$

Furthermore, we can express M_C as the sum of two components: a non-time dependent M_{C1} that is a systematic contamination and can be expressed as a percentage of the total background mass sampled with M_{C1} = aM_B (a = constant); a time dependent M_{C2} that is proportional to the collection time, Δt, and governed by a contamination rate C (expressed in mg/min and due to leakages in the RPO, reasonable to assume where vacuum fittings were used in a non-vacuum system) with M_{C2} = Δt C. With this, (3) can be re-arranged to:

$$\begin{aligned} F^{14}C_B &= F^{14}C_D + \frac{M_{C1} + M_{C2}}{M_B} (F^{14}C_C - F^{14}C_D) \\ F^{14}C_B &= F^{14}C_D + \frac{aM_B}{M_B} (F^{14}C_C - F^{14}C_D) + \frac{\Delta}{M_B} (F^{14}C_C - F^{14}C_D) \\ F^{14}C_B &= (F^{14}C_D + a\Delta F) + \frac{\Delta}{M_B} \Delta F \end{aligned} \tag{4}$$

where ΔF = F¹⁴C_C - F¹⁴C_D

This is equivalent to the linear expression:

$$y = c + mx$$

where y = F¹⁴C_B, c = F¹⁴C_D + aΔF, m = CΔF, x = $\frac{\Delta t}{M_B}$

As we measure F¹⁴C_B, Δt, and M_B, we used the above relationship to apply a linear regression (ordinary least squares carried out with MATLAB R2020a, Figure 2) on our background dataset and established estimates of c and m that were then used to estimate an F¹⁴C value for background corrections on all samples.

The associated uncertainty in the background correction, δ_B, using the uncertainties in c and m, δ_c and δ_m, respectively, calculated from regression analysis, can be expressed as,

$$\delta_B^2 = \left(\frac{\partial y}{\partial c}\right)^2 \delta_c^2 + \left(\frac{\partial y}{\partial m}\right)^2 \delta_m^2 + \left(\frac{\partial y}{\partial x}\right)^2 \delta_x^2$$

$$\delta_B^2 = \delta_c^2 + \left(\frac{\Delta t}{M_B}\right)^2 \delta_m^2 + m^2 \delta_x^2 \quad (5)$$

This also includes an expression for the uncertainty in $x = \frac{\Delta t}{M_B}$, δ_x^2 . This is given by:

$$\left(\frac{\delta_x}{x}\right)^2 = \left(\frac{\delta \Delta t}{\Delta t}\right)^2 + \left(\frac{\delta M_B}{M_B}\right)^2$$

$$\delta_x^2 = \left(\frac{\Delta t}{M_B}\right)^2 \left(\left(\frac{\delta \Delta t}{\Delta t}\right)^2 + \left(\frac{\delta M_B}{M_B}\right)^2 \right) \quad (6)$$

with $\frac{\delta \Delta t}{\Delta t}$ the fractional uncertainty in the measurement of the duration of CO₂ capture for a temperature fraction and $\frac{\delta M_B}{M_B}$ the fractional uncertainty in the estimated mass of gas captured. The uncertainties in the measured duration of capture, $\delta \Delta t$, and mass of gas captured, δM_B , are 10 seconds and 0.02 mg, respectively.

The above methodology was applied to the RPO background dataset resulting in an estimate to be used in future background corrections. The parameters of this model will be updated regularly with 1–2 new background runs for every 6–8 sample runs.

RESULTS AND DISCUSSION

Backgrounds

The results from all backgrounds are presented in Figure 3 with the associated ages shown in Table 1. The average background value is $F^{14}C = 0.0075 \pm 0.0032$ (39950 ± 3132 BP, $n = 44$). No significant differences were observed between anthracite and calcite results. Background $F^{14}C$ values are consistent with contamination ranging from approximately 0.2–0.8% modern CO₂. From our regression analysis the contamination not associated with leakage into the RPO line, i.e., systematic contamination, results in $F^{14}C = 0.0049 \pm 0.0008$, corresponding to an age of 42,700 years BP (approximately 0.25% modern carbon). Any remaining contamination is most likely derived from RPO/RC line leakages. We assume the dominant source of such leakages are connections between Swagelok Ultra-Torr vacuum fittings and the quartz glass at the entrance and exit of the furnace that are prone to low-level leakages when operating under non-vacuum conditions.

Figure 4 shows CO₂ profiles of CO₂ captured fractions and associated ages of anthracite (4a) and calcite (4b) RPO runs. These demonstrate the statistical agreement observed between the ages obtained from different temperature fractions. The profiles are as expected; a broad shoulder of thermal decomposition (approximately 550–950°C) is evident on the anthracite profile and a well-defined peak (approximately 650–850°C) of thermal decomposition (795°C) is seen on the calcite profile. Both profiles indicate that the RPO/RC system is efficient at the upper limit of its temperature range (< 1000°C). The yields obtained on complete runs (i.e., RPO runs to high enough temperatures to allow complete thermal decomposition) were also in good agreement with expected values: for anthracite two complete runs each resulted in a yield of % C = 93%; for spar calcite seven complete runs resulted in yields of % C = 12.9 ± 1.5%. Yields in agreement with expected values, particularly for high carbon content anthracite, support that the RPO system is completely oxidizing and capable of capturing all the pyrolysis products produced in the process.

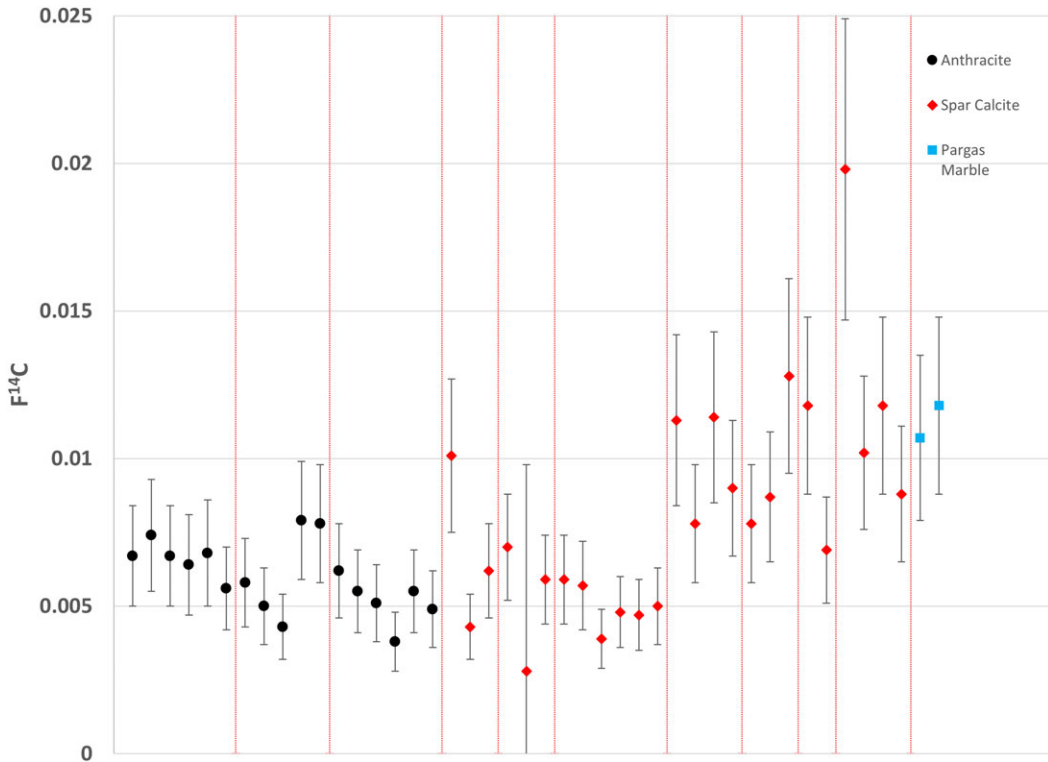


Figure 3 RPO background results (1σ) expressed in $F^{14}C$. Note apparent shift to more modern values is associated with the use of smaller samples sizes, longer collection times, and an associated higher proportion of contamination. Black circle—anthracite; red diamond—spar calcite; blue square—Pargas marble. Red vertical lines used to separate individual RPO runs.

Secondary Standards

The results of secondary standards TIRI-B and ANU Sucrose are presented in Tables 2 and 3 and the associated radiocarbon age and $F^{14}C$ results are plotted in Figure 5. An example RPO run for each is presented in Figure 6. The results are within range of consensus values. The mean age of TIRI-B samples was 4482 ± 47 years BP ($N = 13$, consensus = 4508 years BP). The mean age of IAEA-C6 ANU Sucrose was $F^{14}C = 1.5036 \pm 0.0034$ ($N = 10$, consensus $F^{14}C = 1.503$). The yield from two complete runs was $\%C = 48.4 \pm 3.0\%$, supporting complete oxidation of the pyrolysis products.

During the pyrolysis of organic material, there is preferential loss of hydrogen, nitrogen, sulphur and oxygen (Li et al. 2013; Williams et al. 2014). This leads to the increased formation of aromatic hydrocarbons, which are more resistant to thermal decomposition. This process is known as charring (Currie et al. 2005; Fernandez et al. 2014; Williams et al. 2014). Charred products decompose at a higher temperature and can leading to double peaks similar to those observed in both the ANU sucrose and TIRI-B pine cellulose CO_2 profiles. Alternatively organic material also comprises multiple carbon pools and the multiple peaks in profiles from this study may indicate the presence of carbon products from different thermal decomposition processes (Hemingway et al. 2017), e.g., sucrose comprises fructose, glucose, which can break down at different temperatures.

Table 1 RPO background results for anthracite, spar calcite, and Pargas marble.

Sample type	Lab identifier	Temp. range (°C)	Mass (mg)	$\Delta t/M$ (min/mg)	^{14}C age (years BP)	σ (years BP)	$F^{14}\text{C}$	σ ($F^{14}\text{C}$)	
Anthracite	41861	652–664	1.12	3.99	40222	2403	0.0067	0.0017	
	41864	652–665	1.12	3.99	39414	2399	0.0074	0.0019	
	41862	700–710	1.16	3.19	40198	2407	0.0067	0.0017	
	41865	700–710	1.16	3.19	40539	2397	0.0064	0.0017	
	41863	900–916	1.16	5.16	40028	2396	0.0068	0.0018	
	41866	900–916	1.16	5.16	41680	2408	0.0056	0.0014	
	41874	650–659	1.16	2.74	41371	2406	0.0058	0.0015	
	41876	700–709	1.24	2.59	42494	2398	0.005	0.0013	
	41877	700–709	1.24	2.59	43794	2402	0.0043	0.0011	
	41878	900–904	1.12	1.25	38908	2391	0.0079	0.002	
	41879	900–904	1.12	1.25	38996	2389	0.0078	0.002	
	41992	651–670	1.08	6.14	40793	2418	0.0062	0.0016	
	41993	651–670	1.08	6.14	41786	2401	0.0055	0.0014	
	41994	700–712	1.1	3.82	42453	2423	0.0051	0.0013	
	41995	700–712	1.1	3.82	44765	2411	0.0038	0.001	
	41996	900–910	1.12	3.08	41734	2406	0.0055	0.0014	
	41997	900–910	1.12	3.08	42664	2399	0.0049	0.0013	
	Spar calcite	41998	700–717	0.64	9.92	36887	2387	0.0101	0.0026
		41999	801–809	1.1	2.70	43700	2393	0.0043	0.0011
42000		815–820	0.96	2.03	40817	2389	0.0062	0.0016	
42010		754–766	0.94	4.24	39882	2390	0.007	0.0018	
42011		800–815	2.02	2.45	47266	2464	0.0028	0.007	
42012		830–840	1.1	3.02	41172	2392	0.0059	0.0015	
42017		700–719	1.02	7.91	41218	2401	0.0059	0.0015	
Spar calcite		42018	700–719	1.02	7.91	41468	2399	0.0057	0.0015
	42019	800–805	1.08	1.91	44528	2420	0.0039	0.001	
	42020	800–805	1.08	1.91	42945	2397	0.0048	0.0012	
	42021	819–827	1.08	3.12	43104	2407	0.0047	0.0012	
	42022	819–827	1.08	3.12	42526	2397	0.005	0.0013	
	42019-2	700–732	0.5	1.17	35999	2385	0.0113	0.0029	
	42019-3	750–771	0.64	1.80	38953	2385	0.0078	0.002	

Table 1 (Continued)

Sample type	Lab identifier	Temp. range (°C)	Mass (mg)	$\Delta t/M$ (min/mg)	^{14}C age (years BP)	σ (years BP)	$F^{14}\text{C}$	σ ($F^{14}\text{C}$)
	42019-4	800–830	0.6	7.77	35903	2383	0.0114	0.0029
	42019-5	836–863	0.5	4.35	37811	2386	0.009	0.0023
	42019-6	700–752	0.42	6.64	38975	2387	0.0078	0.002
	42019-7	800–820	0.58	6.87	38142	2388	0.0087	0.0022
	42019-8	850–880	0.94	13.13	35012	2382	0.0128	0.0033
	42019-9	815–840	0.78	3.45	35635	2388	0.0118	0.003
	42019-10	863–880	0.7	3.26	39940	2391	0.0069	0.0018
	42019-12	710–726	0.36	6.39	31489	2381	0.0198	0.0051
	42019-13	737–755	0.52	4.79	36868	2387	0.0102	0.0026
	42019-14	765–775	0.58	13.24	35676	2386	0.0118	0.003
	42019-15	786–796	0.62	10.38	38001	2387	0.0088	0.0023
Pargas marble	42493	780–786	1	5.17	36424	2389	0.0107	0.0028
	42494	750–757	0.76	4.78	35627	2385	0.0118	0.003
					Mean $F^{14}\text{C}$		0.0075	
					Standard deviation		0.0032	
					Mean age (^{14}C years BP)		39345	
					1 σ age range (^{14}C years BP)		36497	43800

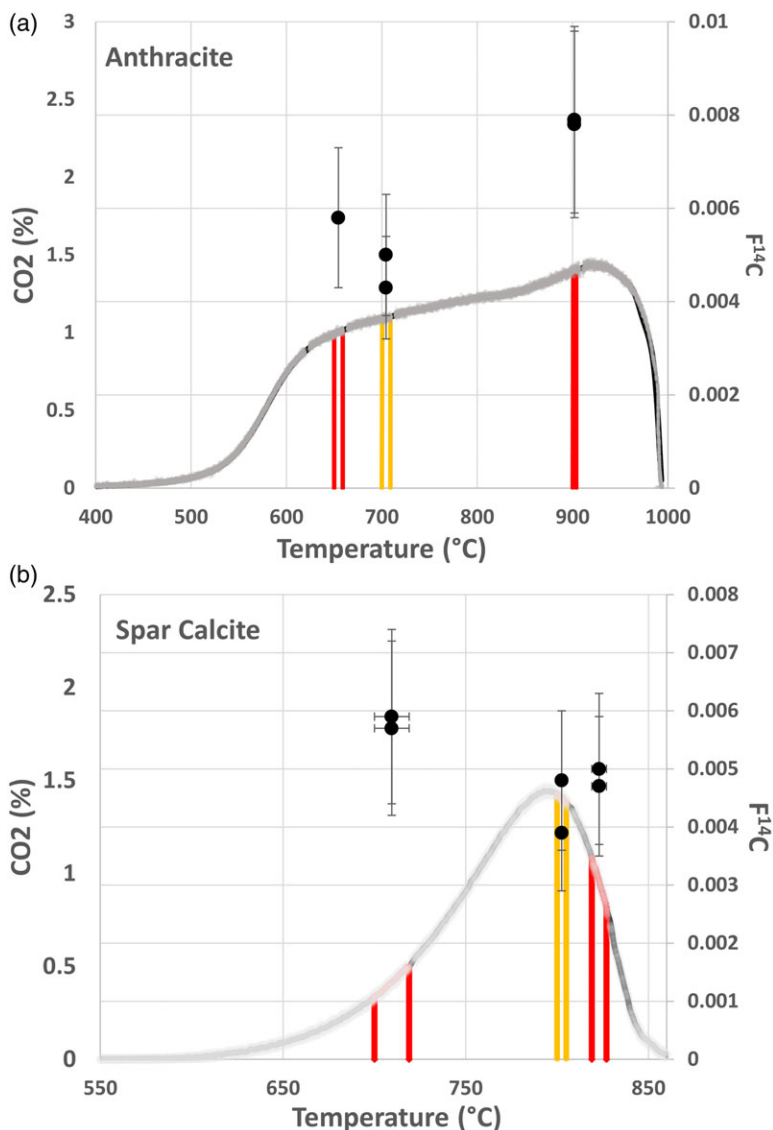


Figure 4 Example background RPO run for anthracite sample (a) and spar calcite sample (b). Fuzzy grey line—raw data (spiked structures associated with valve sequence switch-over have been removed). Black solid line—spline smoothed data. Red and yellow boundaries mark temperature intervals of CO₂ capture with resultant radiocarbon results (F¹⁴C) presented on secondary axis (y axis error bars to 1 σ , x axis error bars mark temperature interval). Duplicates of the CO₂ fraction captured were dated for most fractions (for anthracite, the duplicates of the last sample are almost identical and difficult to distinguish).

However, this highlights a potential issue with RPO of organic samples, as low temperature pyrolysis products may char and become resistance to thermal decay leading to decomposition at higher temperatures. Organic samples may contain a mixture of carbon sources. Labile carbon can form char and evolve at the equivalent temperatures to older

Table 2 RPO results from TIRI-B Pine.

Lab ID	Temperature range (°C)	Mass (mg)	F ¹⁴ C	σ (F ¹⁴ C)	¹⁴ C age (years BP)	σ (years BP)
Run 1						
UBA-42126	295–320	0.62	0.5759	0.0027	4433	37
UBA-42127	325–333	1.02	0.5707	0.0021	4506	29
UBA-42128	350–361	1.06	0.5681	0.0018	4543	26
UBA-42129	419–440	0.98	0.5779	0.0019	4406	26
Run 2						
UBA-42270	320–325	0.98	0.5699	0.0016	4517	22
UBA-42271	341–350	1.54	0.5667	0.0016	4562	22
UBA-42272	341–350	1.54	0.5746	0.0016	4451	22
UBA-42273	394–400	0.7	0.5752	0.0016	4443	22
Run 3						
UBA-42273-6	300–312	0.46	0.5702	0.0019	4513	27
UBA-42273-7	331–337	0.64	0.5714	0.0015	4496	21
UBA-42273-8	348–365	1.08	0.5734	0.0017	4468	24
UBA-42273-9	432–460	0.44	0.5759	0.0026	4433	36
UBA-42273-11	560–574	0.58	0.5709	0.0018	4502	26
Mean F ¹⁴ C	0.5724 ± 0.0034					
Mean age (years BP)	4482 ± 47					
Consensus age (years BP)	4508					

Table 3 RPO results for IAEA-C6 ANU-Sucrose.

Lab ID	Temperature range (°C)	Mass (mg)	F ¹⁴ C	σ (F ¹⁴ C)
Run 1				
UBA-42123	220–234	0.62	1.4974	0.0033
UBA-42124	263–272	0.96	1.5039	0.0034
UBA-42125	300–319	1.68	1.5014	0.0030
Run 2				
UBA-42254	275–293	1.02	1.4996	0.0023
Run 3				
UBA-42496	330–353	1	1.5039	0.0034
UBA-42498	545–574	0.68	1.508	0.0035
UBA-42499	700–735	1.08	1.506	0.0032
Run 4				
UBA-42254-2	249–266	0.42	1.5052	0.0050
UBA-42254-5	545–571	0.52	1.5031	0.0030
UBA-42254-6	600–619	0.62	1.5076	0.0032
Mean F ¹⁴ C	1.5036 ± 0.0034			
Consensus F ¹⁴ C	1.503			

recalcitrant carbon. As such, this may lead to incorporation of this labile material into the high temperature fraction; the high temperature fraction ¹⁴C age will consequently be offset and appear younger. Either a charring correction (Williams et al. 2014) or utilization of ramped

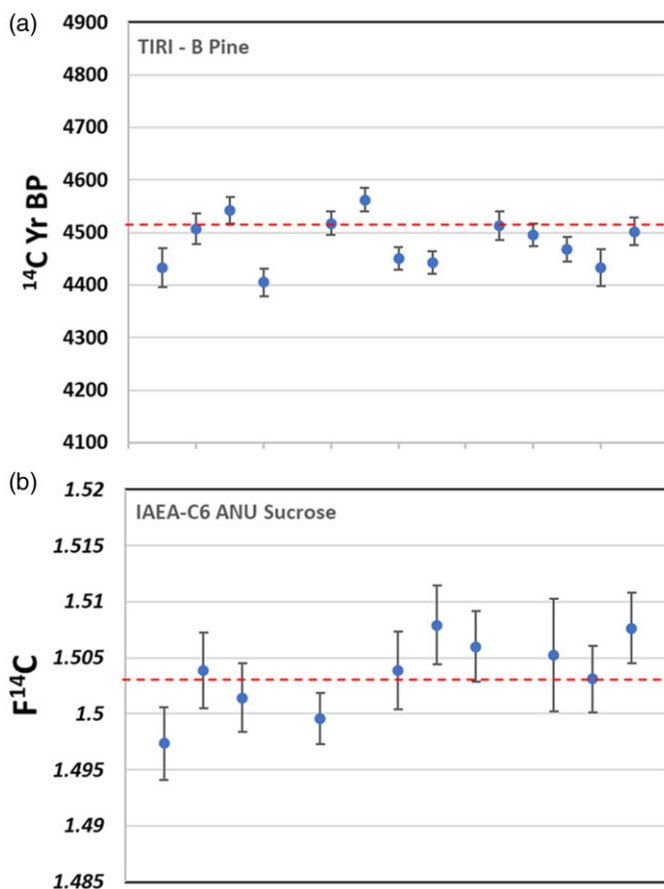


Figure 5 RPO results from analysis of TIRI – B pine (a) and IAEA-C6 ANU Sucrose (b). Red dashed line—consensus value, ^{14}C age = 4508 years BP (pine) and $F^{14}\text{C}$ = 1.503 (sucrose). Error bars to 1σ .

combustion may be more appropriate for some organic samples (the RPO/RC system at the ^{14}C HRONO Centre is equipped to perform both procedures), especially where higher temperature fractions are of interest.

CONCLUSION

Backgrounds and secondary standard CO_2 profiles and radiocarbon values presented here demonstrate the ability of the ^{14}C HRONO Ramped Pyrooxidation line to measure varying sample types with an acceptable process background value. Future testing will include the operation of the ramped combustion mode and collection of CO_2 for $\delta^{13}\text{C}$ stable isotope analysis. The efficacy of this RPO/RC facility has been tested using a range of sample types including mortar, lake and marine sediment, and a preserved archaeological wooden bowl from the National Museum, Dublin (Ireland). Publication of these results is forthcoming. The results of background and standard results here give us confidence that our analyses are robust and replicable.

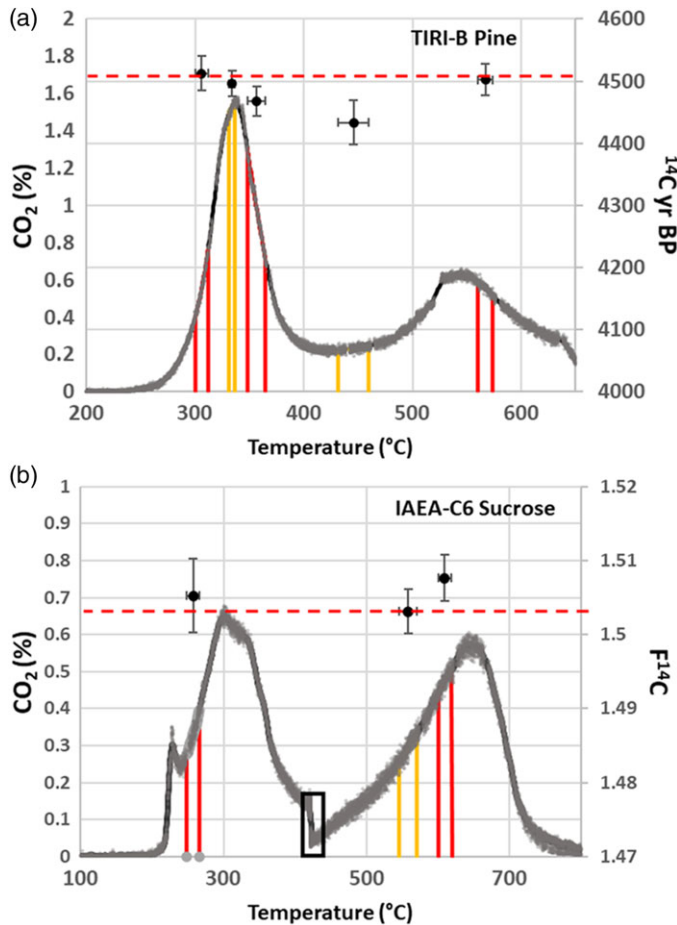


Figure 6 Example RPO run for TIRI-B pine sample (a) and IAEA C-6 ANU Sucrose (b). Fuzzy gray line—raw data (spiked structures associated with valve sequence switch-over removed). Black solid line—spline smoothed data. Red and yellow boundaries mark temperature intervals of CO₂ capture with resultant radiocarbon results presented on secondary axis (y axis error bars to 1σ , x axis error bars mark temperature interval). Dashed red line—consensus value of (age = 4508 years BP and $F^{14}C = 1.504$, respectively). Black solid region—run paused to resolve ice trap blockage.

ACKNOWLEDGMENTS

We would like to thank our colleagues at NOSAMS and the University of South Florida, in particular Brad Rosenheim, Prosper Zigah, Ann McNichol, and Mary Lardie, for all their generous advice and guidance. We also would like to express our gratitude to George Burton and Ben Healey (Queen's University Belfast) for glassware manufacture and their assistance with glassware design. For electronics advice, we also wish to thank Barry Finnegan for his assistance. We also want to thank Jordon Hemingway and an anonymous reviewer for constructive comments. Finally, a thanks to the broader ¹⁴CHRONO team and the School of Natural and Built Environment for their on-going assistance and support.

REFERENCES

- Bao R, McNichol AP, McIntyre CP, Xu L, Eglinton TI. 2018. Dimensions of radiocarbon variability within sedimentary organic matter. *Radiocarbon* 60(3):775–790.
- Currie, LA, Kessler, JD. 2005. On the isolation of elemental carbon for micro-molar ^{14}C accelerator mass spectrometry; evaluation of alternative isolation procedures, and accuracy assurance using a hybrid isotopic particulate carbon reference material. *Atmospheric Chemistry and Physics* 5: 2833–2845
- Fernandez A, Santos GM, Williams EK, Pendergraft MA, Vetter L, Rosenheim BE. 2014 Blank corrections for ramped pyrolysis radiocarbon dating of sedimentary and soil organic carbon. *Analytical Chemistry* 86(24):12085–12092.
- Grimm EC, Maher LJ, Nelson DM. 2009. The magnitude of error in conventional bulk-sediment radiocarbon dates from central North America. *Quaternary Research* 72(2):301–308.
- Hemingway JD, Galy VV, Gagnon AR, Grant KE, Rosengard SZ, Soulet G, Zigah PK, McNichol AP. 2017. Assessing the blank carbon contribution, isotope mass balance, and kinetic isotope fractionation of the ramped pyrolysis/oxidation instrument at NOSAMS. *Radiocarbon* 59(1): 179–193.
- Hemingway JD, Rothman DH, Rosengard SZ, Galy VV. 2017. An inverse method to relate organic carbon reactivity to isotope composition from serial oxidation. *Biogeosciences* 14(22).
- Higham TF. 2019. Removing contaminants: a restatement of the value of isolating single compounds for AMS dating. *Antiquity* 93(370): 1072–1075.
- Hughes IG, Hase TPA. 2009. *Measurements and their uncertainties: a practical guide to modern error analysis*. New York: Oxford University Press. p. 27.
- Keaveney EM, Reimer PJ, Foy RH. 2015. Young, old, and weathered carbon-part 1: using radiocarbon and stable isotopes to identify carbon sources in an alkaline, humic lake. *Radiocarbon* 57(3):407–423.
- Li X, Shen Q, Zhang D, Mei X, Ran W, Xu Y, Yu G. 2013. Functional groups determine biochar properties (pH and EC) as studied by two-dimensional ^{13}C NMR correlation spectroscopy. *PLoS One* 8(6).
- Manning MP, Reid RC. 1977. CHO systems in the presence of an iron catalyst. *Industrial & Engineering Chemistry Process Design and Development* 16(3):358–361.
- Reimer PJ, Brown TA, Reimer RW. 2004. Discussion: reporting and calibration of post-bomb ^{14}C data. *Radiocarbon* 46(3):1299–1304.
- Rosenheim BE, Day MB, Domack E, Schrum H, Benthien A, Hayes JM. 2008. Antarctic sediment chronology by programmed-temperature pyrolysis: methodology and data treatment. *Geochemistry, Geophysics, Geosystems* 9(4).
- Rosenheim BE, Santoro JA, Gunter M, Domack GW. 2013. Improving Antarctic sediment ^{14}C dating using ramped pyrolysis: an example from the Hugo Island Trough. *Radiocarbon* 55: 115–126.
- Suiver M, Polach HA. 1977. Discussion: reporting of C-14 data. *Radiocarbon* 19:355–363.
- van der Plicht J, Hogg A. 2006. A note on reporting radiocarbon. *Quaternary Geochronology* 1(4): 237–240.
- van der Plicht J, Palstra SW. 2016 Radiocarbon and mammoth bones: what's in a date. *Quaternary International* 406:246–251.
- Vogel JS, Nelson DE, Southon JR. 1987. ^{14}C background levels in an accelerator mass spectrometry system. *Radiocarbon* 29(3):323–333.
- Williams EK, Rosenheim BE, McNichol AP, Masiello CA. 2014 Charring and non-additive chemical reactions during ramped pyrolysis: applications to the characterization of sedimentary and soil organic material. *Organic geochemistry* 77:106–114.
- Zigah PK, Minor EC, McNichol AP, Xu L, Werne JP. 2017 Constraining the sources and cycling of dissolved organic carbon in a large oligotrophic lake using radiocarbon analyses. *Geochimica et Cosmochimica Acta* 208:102–118.